

ADVANCED MATERIALS

Supporting Information

for *Adv. Mater.*, DOI: 10.1002/adma.201502969

Charge-Carrier Dynamics and Mobilities in Formamidinium
Lead Mixed-Halide Perovskites

*Waqas Rehman, Rebecca L. Milot, Giles E. Eperon,
Christian Wehrenfennig, Jessica L. Boland, Henry J. Snaith,
Michael B. Johnston, and Laura M. Herz**

Supporting Information

Charge-Carrier Dynamics and Mobilities in Formamidinium Lead Mixed-Halide Perovskites

Waqas Rehman, Rebecca L. Milot, Giles E. Eperon, Christian Wehrenfennig, Jessica L. Boland, Henry J. Snaith, Michael B. Johnston and Laura M. Herz*

A. Sample preparation

1. Perovskite precursor synthesis

Formamidinium iodide (FAI) and formamidinium bromide (FABr) were synthesised by dissolving formamidinium acetate powder in a 1.5x molar excess of 57% w/w hydroiodic acid (for FAI) or 48% w/w hydrobromic acid (for FABr). After addition of acid, the solution was left stirring for 10 minutes at 50°C. Upon drying at 100°C, a yellow-white powder was formed. This was then washed with diethyl ether and recrystallized with ethanol to form white needle-like crystals. Before use, it was dried overnight in a vacuum oven.

To form FAPbI₃ and FAPbBr₃ precursor solutions, FAI and PbI₂ or FABr and PbBr₂ were dissolved in anhydrous N,N-dimethylformamide (DMF) in a 1:1 molar ratio at 0.55 M of each reagent to give a 0.55 M perovskite precursor solution.

2. Film formation

Immediately prior to film formation, small amounts of acid were added to the stock precursor solutions to enhance the solubility of the precursors and allow smooth and uniform film formation. To 1 ml of the 0.55 M FAPbI₃ precursor solution, 38 µl of hydroiodic acid (57%w/w) was added, and 32 µl of hydrobromic acid (48%w/w) was added to 1 ml of the 0.55 M FAPbBr₃ precursor solution.

To form the $\text{FAPb}(\text{Br}_y\text{I}_{1-y})_3$ perovskite precursors, mixtures were made of the FAPbI_3 and FAPbBr_3 solutions in the required ratios after the addition of acid. Films were then spin-coated on warm (85°C) z-cut quartz substrates at 2000 rpm in a nitrogen-filled glovebox and subsequently annealed in air at 170°C for 10 minutes. This gave very uniform pinhole-free layers of $\sim 300\text{-}400\text{nm}$ thickness.

B. Absorbance spectra

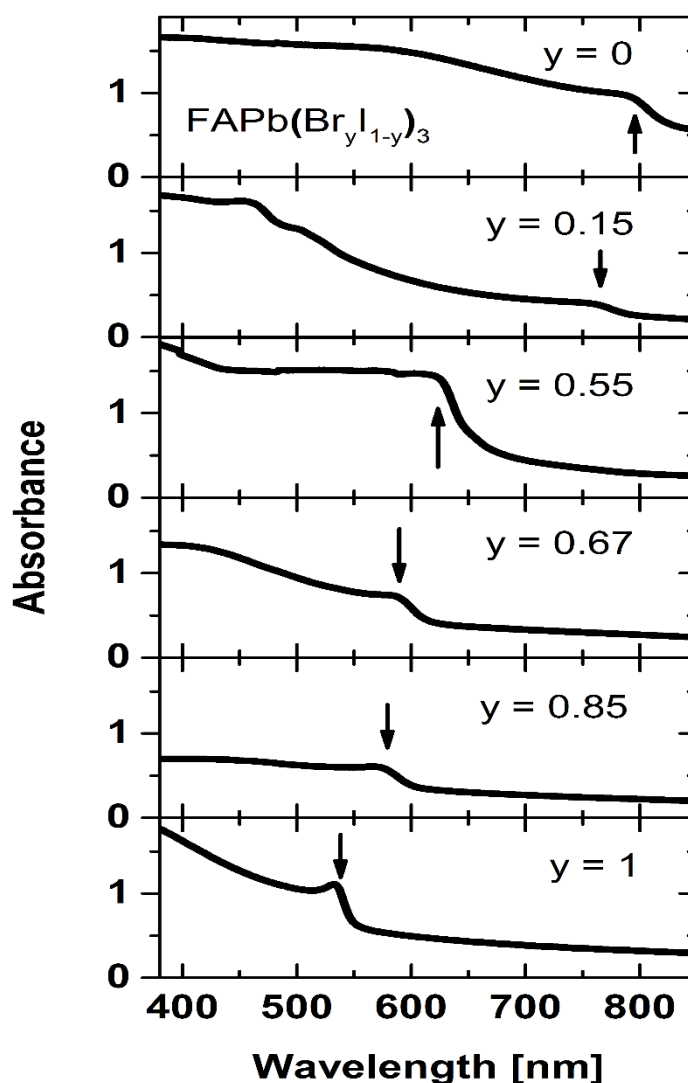


Figure S1. UV-VIS absorbance spectra of $\text{FAPb}(\text{Br}_y\text{I}_{1-y})_3$ films with varying halide composition. Vertical arrows indicate the absorption onsets. The spectra were recorded using a PerkinElmer Lambda 1050 UV/Vis/NIR spectrometer.

C. Optical pump - THz probe spectroscopy

The optical-pump-THz-probe setup uses a Spectra Physics Ti:Sapphire regenerative amplifier to generate 40 fs pulses at a center wavelength of 800 nm and a repetition rate of 1.1kHz. Terahertz pulses were generated by optical rectification in a 450 μm thick GaP(110) single crystal and detected by electro-optic sampling in a ZnTe crystal (0.2mm (110)-ZnTe on 3mm (100)-ZnTe). Pulses for optical excitation of the samples at 400nm have been generated using a beta barium borate crystal for frequency doubling. Optical excitation was carried out from the substrate side of the film. The diameters of optical pump and THz probe beams at the sample position were 3.6 mm and 2.4 mm (FWHM), respectively. Measurements were performed with the entire THz beam path (including emitter, detector and sample) in an evacuated chamber at a pressure of $<10^{-2}$ bar.

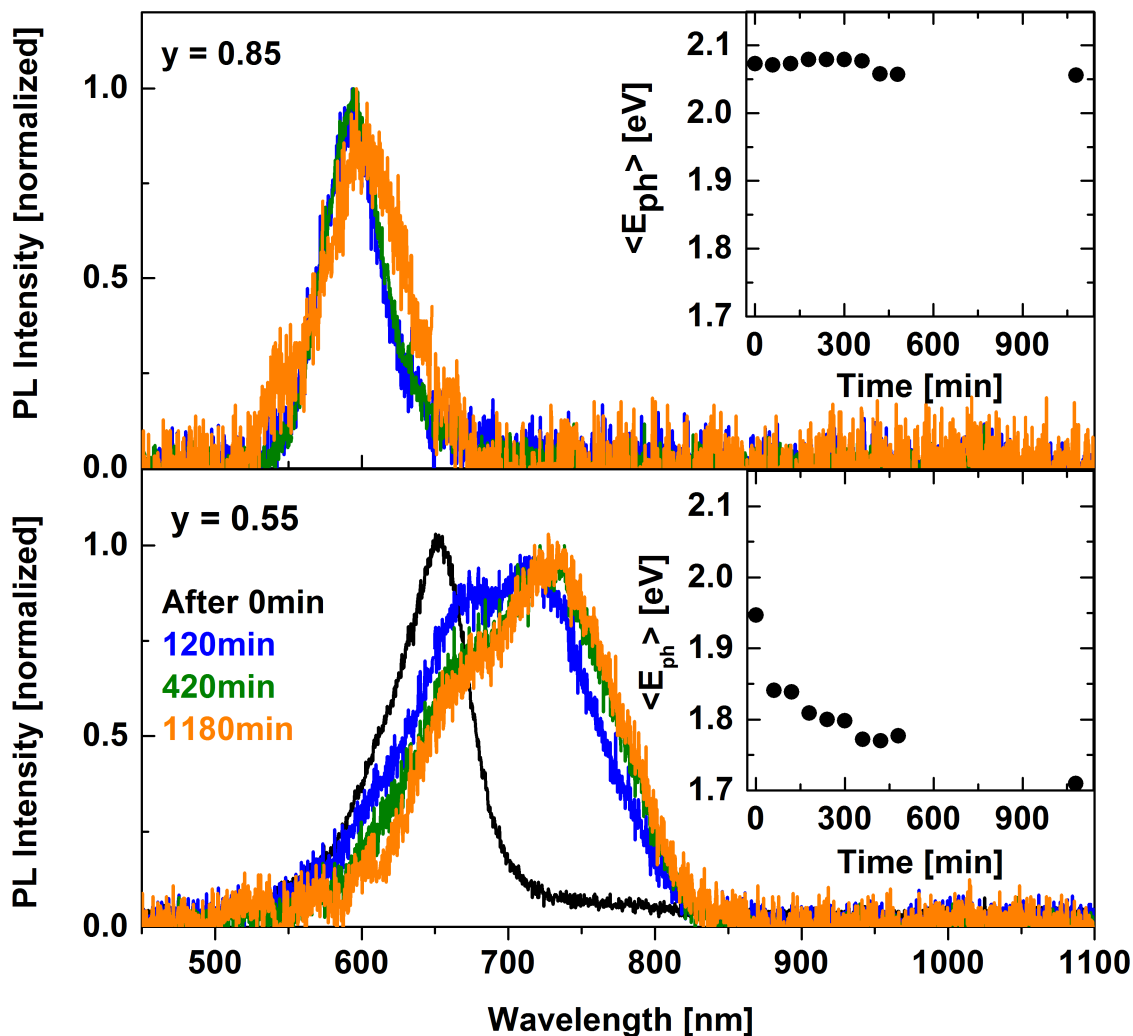
D. In-situ PL of selected bromide-rich FAPb(Br_yI_{1-y})₃ films

Figure S2. In-situ PL spectra of the FAPb(Br_{0.85}I_{0.15})₃ and FAPb(Br_{0.55}I_{0.45})₃ films under continuous excitation at 400 nm for 1180 minutes in an evacuated box (used for THz measurements). The excitation fluence is 13.5 $\mu\text{J cm}^{-2}$ and the excitation intensity is 14.9 mW cm^{-2} . All spectra have been normalized to the peak emission. Insets: Change of the average photon energy $\langle E_{ph} \rangle$ as a function of time.

E. Time-resolved photoluminescence (PL)

Time-resolved PL spectroscopy by means of time-correlated single photon counting (TCSPC) was performed to determine monomolecular recombination rate constants k_1 . A picosecond pulsed diode laser (Picoquant, LDH-D-C-405M) centered at 400 nm was used to photoexcite the sample. The PL was collected and directed toward a grating monochromator (Princeton Instruments, SP-2558) fitted with a photon counting detector (PDM series from MPD). The timing was controlled with a PicoHarp300 time-correlated single photon counting (TCSPC) event timer. Measurements were undertaken at very low excitation fluences where higher order processes are assumed to be negligible. Monomolecular recombination rates k_1 were extracted through mono-exponential fits to the tails of the low-fluence PL decay traces of each film as shown in Figures S3 and largely reflect trap-assisted charge carrier recombination which dominates in the very low charge-carrier density regime. Since PL measurements generally rely on more tightly focused laser beams, even at the low fluences explored the mixed-halide perovskites may be subject to some photoinduced halide segregation effects, as discussed in the main text. The subsequent migration of charge-carriers following such creation of lower-energy inclusions with high iodide content might also cause the observed initial non-exponential decay traces for some of the samples, however, energetic disorder would result in similar effects. While curves were acquired at lowest possible fluences and acquired reasonable quickly, some light-induced segregation may influence the PL traces creating additional error in the extracted monomolecular recombination rates k_1 . However, the bimolecular and Auger rates are determined through THz transient photoconductivity spectroscopy at much lower excitation intensity and are not affected, as discussed in the main text.

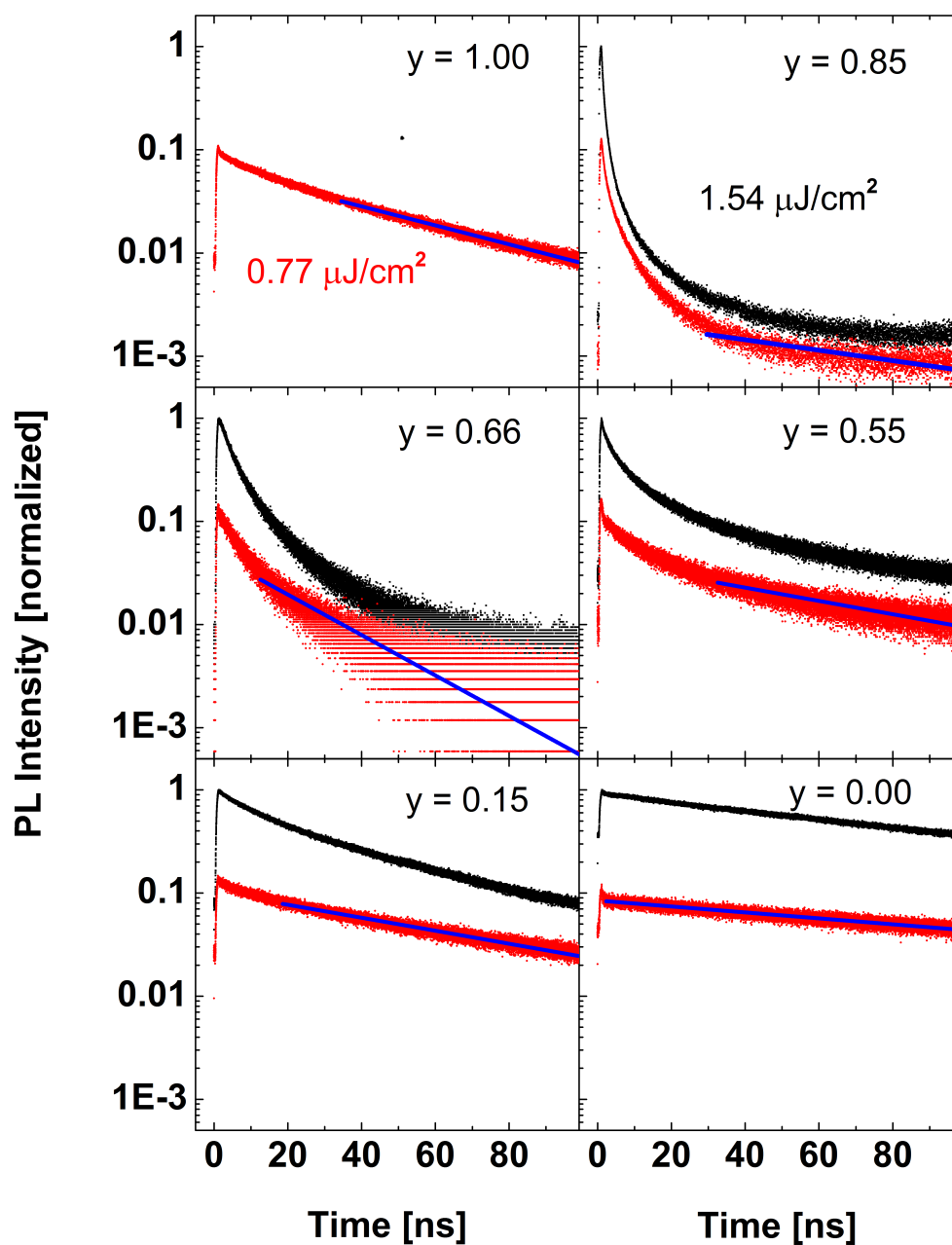


Figure S3. Time-resolved PL spectroscopy of FAPb(Br_yI_{1-y})₃ following excitation at 400 nm with excitation fluences of 0.77 μJ/cm² (red trace) and 1.54 μJ/cm² (black trace). The laser intensity was at 7.77 W/cm² for the lower fluence measurement.

F. Derivation of photoconductivity and charge carrier mobility from change in THz electric field transmission

Assuming the thickness of the perovskite film is smaller than the THz wavelength, the sheet photoconductivity ΔS of a thin film between two media of refractive indices n_a and n_b can be expressed as

$$\Delta S = -\varepsilon_0 c (n_a + n_b) \frac{\Delta T}{T} \quad (1)$$

where the product $\varepsilon_0 c$ denotes the invert of the vacuum impedance and $\Delta T/T$ the photoinduced change in THz electric field transmission over total transmission. As the experiment has been performed in an evacuated box under vacuum, the samples are surrounded by vacuum from one side ($n_b = 1$) and in direct contact with the z-cut quartz substrate from the other side ($n_a = 2.13$) through which the photoexcitation of the sample occurs.

The charge-carrier mobility μ can be calculated as follows

$$\mu = \frac{\Delta S A_{eff}}{N e} \quad (2)$$

where ΔS is the sheet photoconductivity of a thin film, e is the elementary charge and N is the number of photoexcited charge-carriers. A_{eff} is the effective area of the overlap of optical pump and THz probe pulse calculated as follows

$$A_{eff} = \frac{\pi}{\ln(2)} (FWHM_{pump}^2 + FWHM_{probe}^2) \quad (3)$$

The number of photoexcited charge-carriers N can be determined as follows

$$N = \varphi \frac{E\lambda}{hc} (1 - R_{pump}) (1 - T_{pump}) \quad (4)$$

where φ is the ratio of charge-carriers produced following photon absorption, also known as the photon-to-charge branching ratio, which is assumed to be unity. E , is the energy contained in an optical excitation pulse of wavelength λ , R_{pump} is the reflectivity of the sample at normal incidence of the excitation beam, T_{pump} denotes for the portion of pump beam which is transmitted through the sample. As φ is declared unknown, we define an effective mobility $\tilde{\mu} = \varphi\mu$ which can be directly obtained from our experiments

$$\varphi\mu = -\varepsilon_0 c (n_a + n_b) \frac{A_{eff} hc}{E e \lambda (1 - R_{pump}) (1 - T_{pump})} \frac{\Delta T}{T} \quad (5)$$

The ascertained charge-carrier mobility contains contributions from both electrons and holes. Hence, the derived values for mobility represent the sum of electron and hole mobilities. As φ ranges between 0 and 1, the effective mobility describes a lower limit. However, the amorphous phases in $\text{FAPb}(\text{Br}_y\text{I}_{1-y})_3$ films ($0.3 < y < 0.5$) made it difficult to obtain significant THz photoconductivity data. Thus, the determination of the photoconductivity onset value prior to charge recombination is subject to uncertainty.

G. Global Fits to THz photoconductivity transients

The recombination dynamics of the free charge-carrier density $n(t)$ is determined by first, second and third order decay mechanisms and described by the following rate equation, also provided in the main manuscript,

$$\frac{dn(t)}{dt} = -k_3 n^3 - k_2 n^2 - k_1 n \quad (6)$$

The experimentally observed quantity of photoinduced THz transmission change $x(t) = \left(\frac{\Delta T}{T}\right)(t)$ is linearly related to the free charge-carrier in the form of

$$n(t) = \varphi C x(t) \quad (7)$$

Hence, $C = n_0/x(0)$ is the proportionality factor between the immediate THz response $x(0)$ and the initially absorbed photon density n_0 with

$$n_0 = \frac{E \lambda \alpha(\lambda)}{hc A_{eff}} (1 - R_{pump}) \quad (8)$$

which can be derived from pump beam parameters and the absorption coefficient α at our excitation wavelength of 400 nm. If (6) is substituted into (5) we obtain the following relation

$$\begin{aligned} \frac{dn(t)}{dt} &= -C^2 \varphi^2 k_3 x^3 - C \varphi k_2 x^2 - k_1 x \\ &= -A_3 x^3 - A_2 x^2 - A_1 x \end{aligned} \quad (9)$$

with $A_i = C^{i-1} \varphi^{i-1} k_i$. Taking a fluence dependent set of THz photoconductivity transients belonging to a particular film, numerical solutions according equation (8) are fitted simultaneously to all transients. Therefore, there is only one globally optimized value for A_i applied to all fluences. As we can expect a spatially varying charge density profile, our fit routine also considers the exponential charge density profile created by the pump beam. The sample is divided into 50 equally thick slices and the decay function is computed for all of these individually.

H. THz photoconductivity spectra

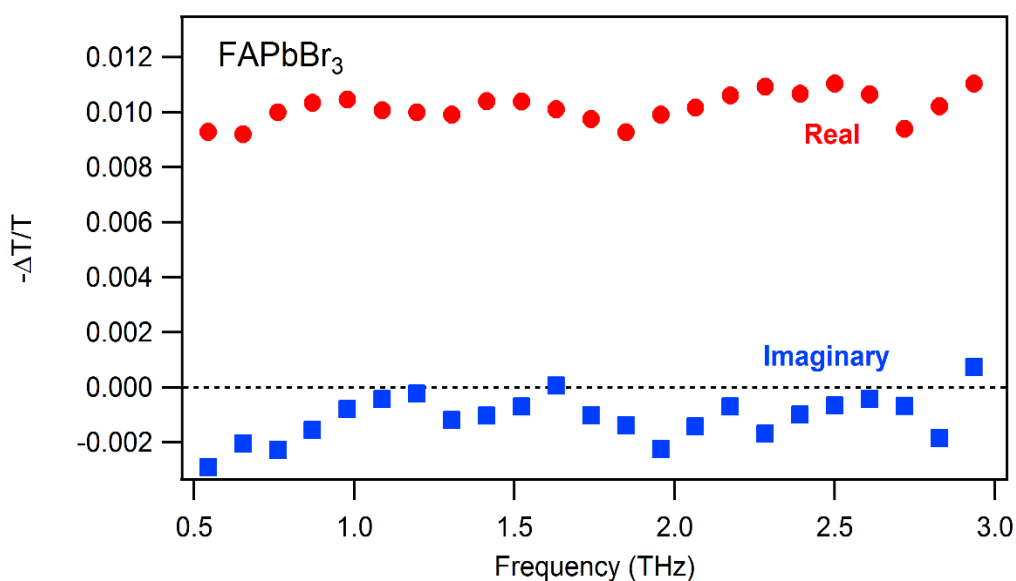


Figure S4. THz photoconductivity spectrum of FAPbBr₃ recorded at a pump-probe delay of 100 ps after excitation at 400 nm with a fluence of 65 μJ cm⁻².

I. Determination of charge-carrier diffusion lengths

In order to further investigate the effects of mobility and recombination rate changes, the diffusion lengths L_D were calculated according to Equation 1.

$$L_D(n) = \sqrt{\frac{D}{R_{total}(n)}} \quad (1)$$

The total recombination rate R_{total} is determined by the charge-carrier density and the recombination rate constants (k_1 , k_2 , and k_3) of the individual recombination processes:

$$R_{total} = -\frac{1}{n} \frac{dn}{dt} = n^2 k_3 + n k_2 + k_1 \quad (2)$$

Here, the diffusion constant D is the product of the mobility μ , Boltzmann constant k_B , and temperature T divided by the elementary charge e :

$$D = \frac{\mu k_B T}{e} \quad (3)$$

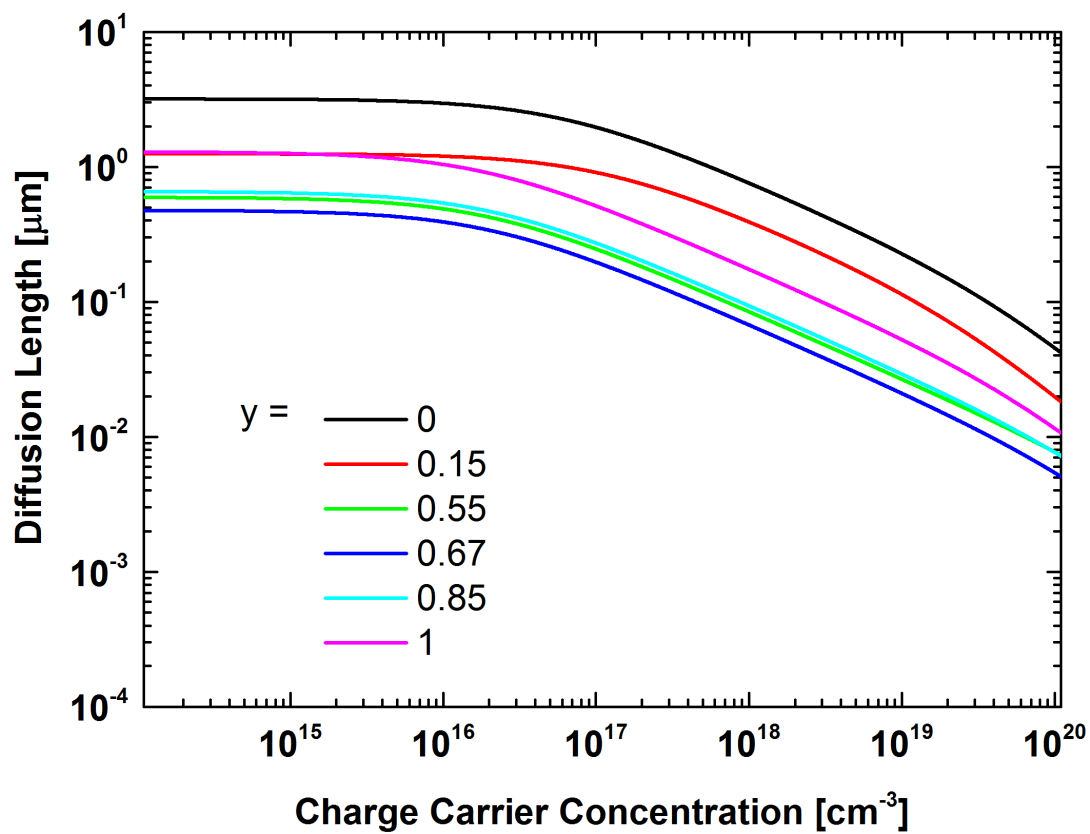


Figure S5. Charge-carrier diffusion lengths as a function of charge-carrier concentration for thin films of $\text{FAPb}(\text{Br}_y\text{I}_{1-y})_3$ with varying bromide content.

J. Table of charge-carrier decay constants and mobility values

Table T1. Column 1: bromide content y of the $\text{FAPb}(\text{Br}_y\text{I}_{1-y})_3$ film. Columns 2 and 3 show the third ($\phi^2 k_3$) and second (ϕk_2) order charge-carrier recombination rate constants extracted from THz photoconductivity transients. Errors displayed for $\phi^2 k_3$ and ϕk_2 were determined from the variation in output of the fitting routine for multiple datasets acquired for the same sample. Errors for k_1 arise mostly from slight deviations of the PL decay data from mono-exponential behaviour, which leads to a dependence of the fitting output on the time window over which data was fitted. Column 4 presents monomolecular recombination rate constants k_1 extracted from monoexponential fits to the PL decay. Column 5 lists the effective charge carrier mobility $\phi\mu$ determined from THz photoconductivity spectroscopy. Column 6 compares the bimolecular-recombination-rate-to-mobility ratio (k_2/μ) to that expected from Langevin theory (subject to factorization with an appropriate value of the dielectric function), and Column 7 lists the diffusion lengths obtained for the low charge-carrier concentration regime ($n=10^{15}\text{cm}^{-3}$).

Perovskite material composition	Charge-carrier decay constants			Effective Mobility	Langevin ratio	Charge-carrier diffusion length at $n=10^{15}\text{cm}^{-3}$
	3 rd order	2 rd order	1 rd order			
$\text{FAPb}(\text{Br}_y\text{I}_{1-y})_3$	$\phi^2 k_3$ ($10^{-28}\text{cm}^6\text{s}^{-1}$)	ϕk_2 ($10^{-9}\text{cm}^3\text{s}^{-1}$)	k_1 (μs^{-1})	$\phi\mu$ ($\text{cm}^2\text{V}^{-1}\text{s}^{-1}$)	$k_2/\mu : e/\epsilon_0$ (10^{-5})	L_d (μm)
$y = 0.00$	0.22 ± 0.05	0.11 ± 0.02	6.7 ± 1	27	0.23	3.14
$y = 0.15$	0.45 ± 0.11	0.13 ± 0.05	14.5 ± 3	9	0.79	1.25
$y = 0.55$	0.39 ± 0.11	1.7 ± 1.1	36 ± 9	5	19.1	0.58
$y = 0.67$	1.6 ± 0.3	2.7 ± 0.8	45 ± 9	5	30.0	0.47
$y = 0.85$	1.5 ± 0.4	2.8 ± 0.7	59 ± 11	10	15.6	0.64
$y = 1.00$	1.5 ± 0.4	1.1 ± 0.3	21 ± 3.0	14	4.52	1.26

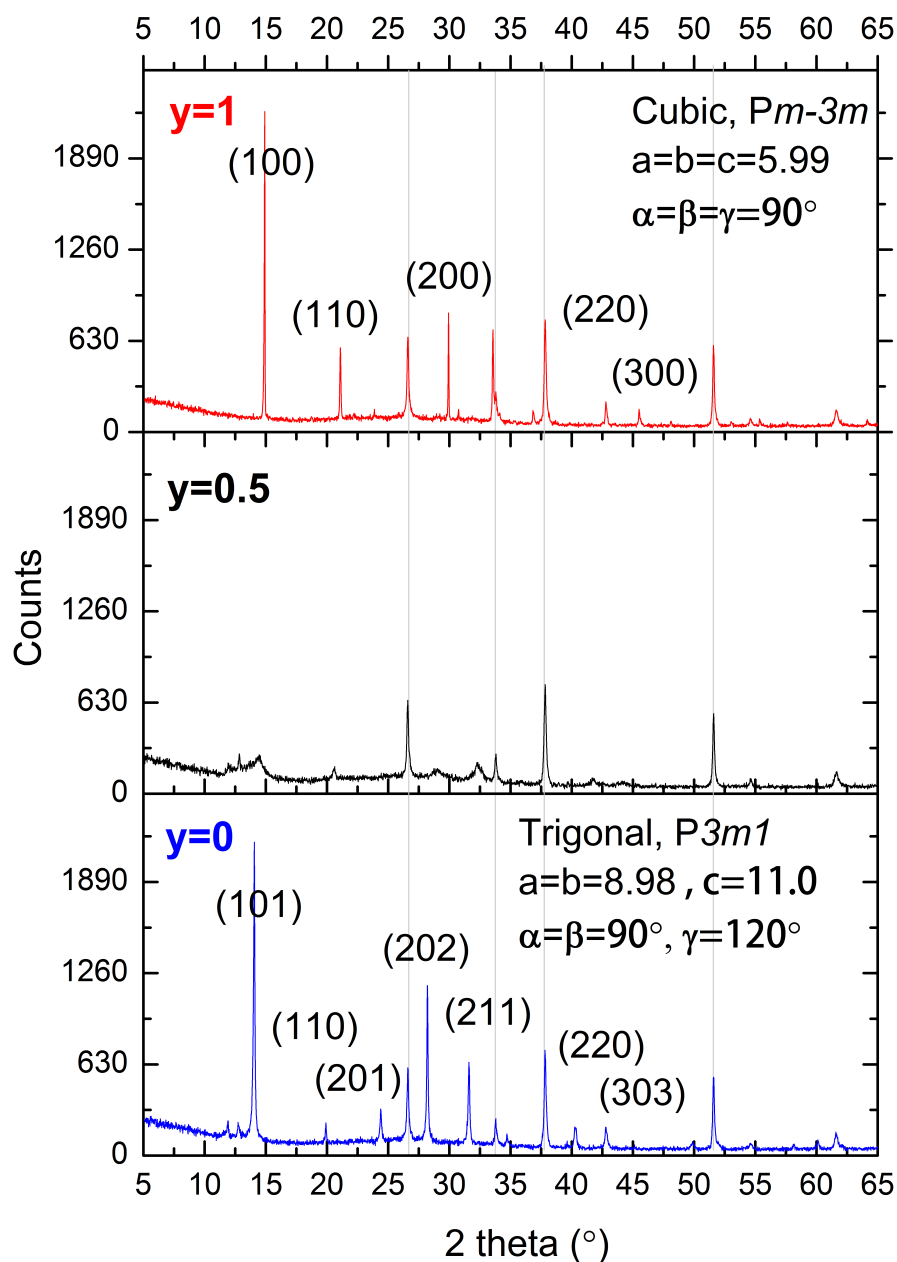
K. XRD Spectra for $\text{FAPb}(\text{Br}_y\text{I}_{1-y})_3$ films

Figure S6. X-ray diffraction (XRD) spectra for FAPbBr_3 ($y=1$), $\text{FAPb}(\text{Br}_{0.5}\text{I}_{0.5})_3$ ($y=0.5$) and FAPbI_3 ($y=0$) with peaks attributed to crystallographic diffraction planes in the perovskite indicated in brackets. The four peaks marked with grey lines arise from the FTO substrate that was present during the measurements.